Nuclear Quadrupole Interactions Studied by Time Differential Perturbed Angular Correlations of γ-Rays *

T. Butz

Universität Leipzig, Fakultät für Physik und Geowissenschaften, Linnéstr. 5, 04103 Leipzig

Z. Naturforsch. **51a**, 396–410 (1996); received December 12, 1995

This paper gives an elementary introduction to time differential perturbed angular correlation of γ-rays emitted from excited nuclei with particular reference to nuclear quadrupole interactions. We start with a comparison to other techniques such as nuclear quadrupole resonance and the Mössbauer effect, quote all necessary formulae, describe a typical spectrometer, list suitable isotopes, and finally give some examples for modern applications.

Key words: Nuclear quadrupole interactions; Time differential perturbed angular correlations (TDPAC); TDPAC: theory, spectrometers, isotopes; Mercury compounds; Tungsten compounds.

1. Introduction

Hyperfine interactions, particularly nuclear quadrupole interactions (NQI), can be studied by a variety of different methods: (i) ultra high resolution atomic spectroscopy which measures energy splittings in the order of neV due to the interaction of atomic electrons with the nuclear moments (magnetic dipole and electric quadrupole moment). Electron paramagnetic resonance also belongs to this class of experiments which look at the "electron" rather than at the "nucleus"; (ii) low temperature static nuclear orientation which detects the unequal population of hyperfine split states at mK-temperatures via the anisotropic emission of γ-rays (or other particles). In principle, the Schottky anomaly in the specific heat at mK-temperatures also belongs to this category of nuclear orientation, although it never gained much importance due to extreme sample purity requirements; (iii) the classical nuclear spectroscopy techniques such as nuclear magnetic resonance (NMR), nuclear quadrupole resonance (NQR), Mössbauer effect (ME) and – the less well known – time differential perturbed angular correlation of γ-rays (TDPAC). In this paper, an elementary introduction to TDPAC is given with particular emphasis on nuclear quadrupole interactions. Although particles other than γ-rays can be used, e.g. α, β-particles or conversion electrons, and although the "on-line" version, namely time differential perturbed angular distributions (TDPAD) in accelerator experiments, play an important role, this paper is restricted to γ-γ-TDPAC.

* Presented at the XIIIth International Symposium on Nuclear Quadrupole Interactions, Providence, Rhode Island, USA, July 23–28, 1995.

Reprint requests to Prof. Dr. T. Butz.

2. TDPAC: Qualitative Introduction

In this section, a qualitative introduction to TDPAC is given, starting with a very simplified discussion of NQR and ME (see Figure 1).

a) NQR

In NQR, the *ground state* of a nucleus which is split due to the NQI is studied. For the sake of simplicity, we assume a spin $I = 3/2$ for this ground state. The NQI-splitting is usually on the order of some neV. Hence, resonance frequencies of $\Delta E/h \sim 10^{-9}$ eV/10^{-15} eVs $\sim$ MHz, i.e. radio frequencies, are required for an absorption by which the population difference between the two split states (which is in the order of 10^{-5} at room temperature) is changed. Very sensitive detection devices are necessary to detect this extremely small absorbed energy. In fact, the number of nuclear spins required in an NQR experiment is typically in the order of 10^{18}. The absorbed energy is transferred to the lattice (or surroundings) described by the spin-lattice relaxation time T_1. The resonance absorption linewidth is governed by the spin-spin relaxation time T_2 and can be very narrow, even in

0932-0784 / 96 / 0500-0396 $ 06.00 © – Verlag der Zeitschrift für Naturforschung, D-72072 Tübingen

solids. Contrary to NMR, where the magnetic field is swept and the resonance is detected at constant frequency, pure NQR does not require the application of an external magnetic field but requires the resonance frequency to be varied, sometimes over quite considerable frequency ranges (say 1–100 MHz). Consequently, sample geometries, filling factors, coils and pickup-coils with frequency dependent Q-factors present considerable difficulties to every NQR experimentalist. In general, the detection of *all* resonances – especially for high spins – and the correct assignment to a specific nucleus are quite difficult tasks. The determination of site populations for samples with several inequivalent sites is hampered by the fact that the T_1 might be quite different on different sites. A major advantage, however, compared to the detection of NQI's in random powder samples by conventional NMR, is the fact that the broad resonance lines due to the *non-collinear* combined magnetic dipolar and electric quadrupolar interactions are avoided.

b) ME

Contrary to NQR, ME does not require radiofrequency (RF) fields. Instead it uses γ-quanta with frequencies in the 10^{18} Hz range, which are emitted by a γ-source (the transmitter) and resonantly absorbed by the sample (the absorber). Needless to say, the transmitter isotope and the absorber isotope have to be identical in order to match the γ-frequency. Provided the emission and the absorption can take place *without recoil* losses – there is a recoilfree fraction whenever the *entire* lattice with a mass in the mg-to-g-range is involved in the emission and absorption process – resonance occurs. For the sake of simplicity, we shall neglect isomer shifts caused by both (i) differences in the mean squared nuclear radius between the ground and excited nuclear states and (ii) differences in the s-electron density at the nuclear site between source and absorber. We also assume a groundstate spin $I = \frac{1}{2}$ (i.e. no splitting) and an excited state spin $I = \frac{3}{2}$, in analogy to the NQR case. The resonant absorption of a γ-quantum yields an excited nuclear state in the absorber which – on the average after a nuclear lifetime τ_N – will re-emit a γ-quantum and return to the groundstate. The resonance linewidth is governed by the nuclear lifetime τ_N. This is typically in the 10–100 ns range, i.e. the linewidth is typically $\Gamma \sim \hbar/\tau_N \sim 10^{-8} \ldots 10^{-7}$ eV. This is, of course, some 10^{11}–10^{12} orders of magnitude smaller than the γ-ray energy. Hence, the ME offers an extremely good energy resolution: it measures energy *differences* between the groundstate and the two slightly different ($\Delta \sim 1$–10 neV) excited nuclear states. There are no particular detection problems and the sensitivity can be rather high, particularly for special variants of the ME: scattering geometries, source experiments (instead of a single-line source and an NQI split absorber an NQI-split source and a single line absorber is used), or conversion electron detection. Frequently, experiments have to be carried out at low temperatures due to small recoil-free fractions at room temperature. The ME provides information on hyperfine splittings and, in addition, on lattice dynamics via the Lamb-Mössbauer factor (recoil-free fraction), a feature which is missing in TDPAC. Relaxation phenomena can be studied both via the phase modulation of the γ-rays and via hyperfine relaxations.

c) TDPAC

The first excited nuclear state is populated by resonant absorption of a γ-quantum from the nucleus in its groundstate in the ME. In TDPAC, it is populated by another higher, excited state, called second excited state in Figure 1. This eliminates the need to have a source (transmitter) and a resonance condition. However, we require a γ-γ-cascade that is fed via the decay of a longlived mother isotope (alternatively, the second excited state could be longlived, i.e. an isomeric state). This means, that the price (energy) to be paid in order to obtain information on the NQI-split system is not in the currency of RF photons or γ-quanta. It usually is provided in a nuclear reaction which creates the unstable mother isotope. In this sense we have a "wound-up spy" which transmits information on its fate while returning to the ground state. Similarly to the ME, the first (intermediate) excited state should have a lifetime in the 10–1000 ns range. This lifetime defines the linewidth, i.e. the energy resolution, in the ME. Similarly, it defines the frequency resolution in TDPAC, as will become clear later. In Fig. 1 we have – for the sake of simplicity – assumed that the second excited state is unsplit and has $I = \frac{1}{2}$, the intermediate state is split and has $I = \frac{3}{2}$, and the ground state is unsplit with $I = \frac{1}{2}$. The-de-excitation of the second excited state may proceed in two ways: either via the upper or via the lower NQI-split intermediate state. Here we have the "classical" quantum mechanical problem of a "black box" with input and output and

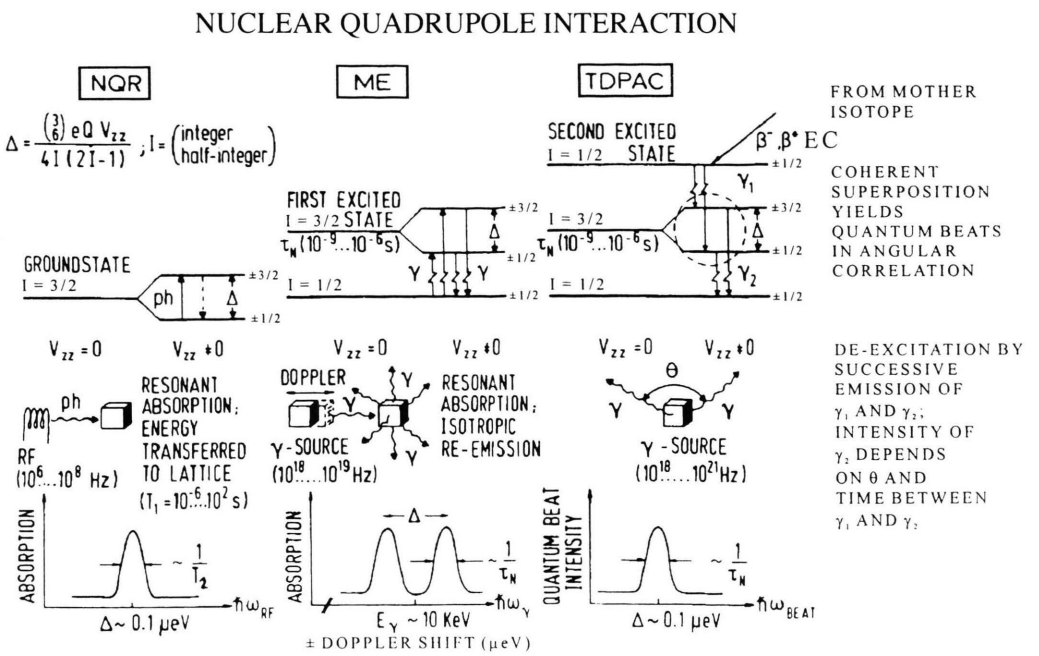

Fig. 1. Schematic comparison of nuclear quadrupole resonance (NQR), Mössbauer effect (ME), and time differential perturbed angular correlation (TDPAC) experiments applied to nuclear quadrupole interactions.

two possible pathways inside the box which are not directly observable. Hence, we have to use a coherent superposition of the amplitudes of both pathways. This leads to quantum beats in the *coincidence* countrate between both quanta with the beat frequency being $\omega = \Delta/\hbar$. Hence, instead of single γ-counts we require a coincidence setup.

In the following, we discuss some basic features of this coincidence experiment. We shall start with a sample with randomly oriented nuclear spins (see Fig. 2, top left). By the mere detection of γ_1 in a given direction we select an aligned subensemble of nuclear spins by virtue of angular momentum conservation: the vectors describing the nuclear spin and its orientation before and after the decay and the vector describing the γ-emission direction and the angular momentum carried away by the quantum have to obey the "triangular rule". This means, that not all nuclei emit γ_1 into the detector 1 with equal probability. Therefore, the emission of a subsequent γ_2 from the same nucleus which already emitted γ_1 into detector 1 will in general depend on the angle between γ_1 and γ_2, i.e. the *coincidence* countrate is anisotropic. In other words, there is an angular correlation between both γ-quanta which is entirely defined by the nuclear spins involved in both transitions and by the multipolarities (and eventually mixing ratios) of both γ-quanta. Note that both *single* countrates for γ_1 and γ_2 do not depend on angles for randomly oriented spins, but their *coincidence* countrate does. Due to parity conservation of the electromagnetic interaction (responsible for the γ-emission), the coincidence probability patterns have *even* multipole orders. The excess (or deficit) of the coincidence countrate at opposite detectors ($\theta = 180°$) compared to the isotropic average is called "anisotropy" (positive for excess and negative for deficit). It would equal the value at an angle $\theta = 0°$, if we could place both detectors at exactly the same position. To lowest order, the angular correlation can be described by an isotropic part and a term proportional to the Legendre polynomial $P_2(\cos\theta)$. For positive anisotropy, we would measure an excess coincidence countrate at $\theta = 180°$ compared to the isotropic rates whereas at $\theta = 90°$ we would measure $-1/2$ of the anisotropy ($P_2(90°) = -1/2$), as depicted in Fig. 2 (middle). This angular correlation can be perturbed by the interaction of nuclear moments with extranuclear fields such as e.g. the nuclear quadrupole moment and the electric field gradient tensor at the nuclear site, which arises from all extranuclear charges. Provided

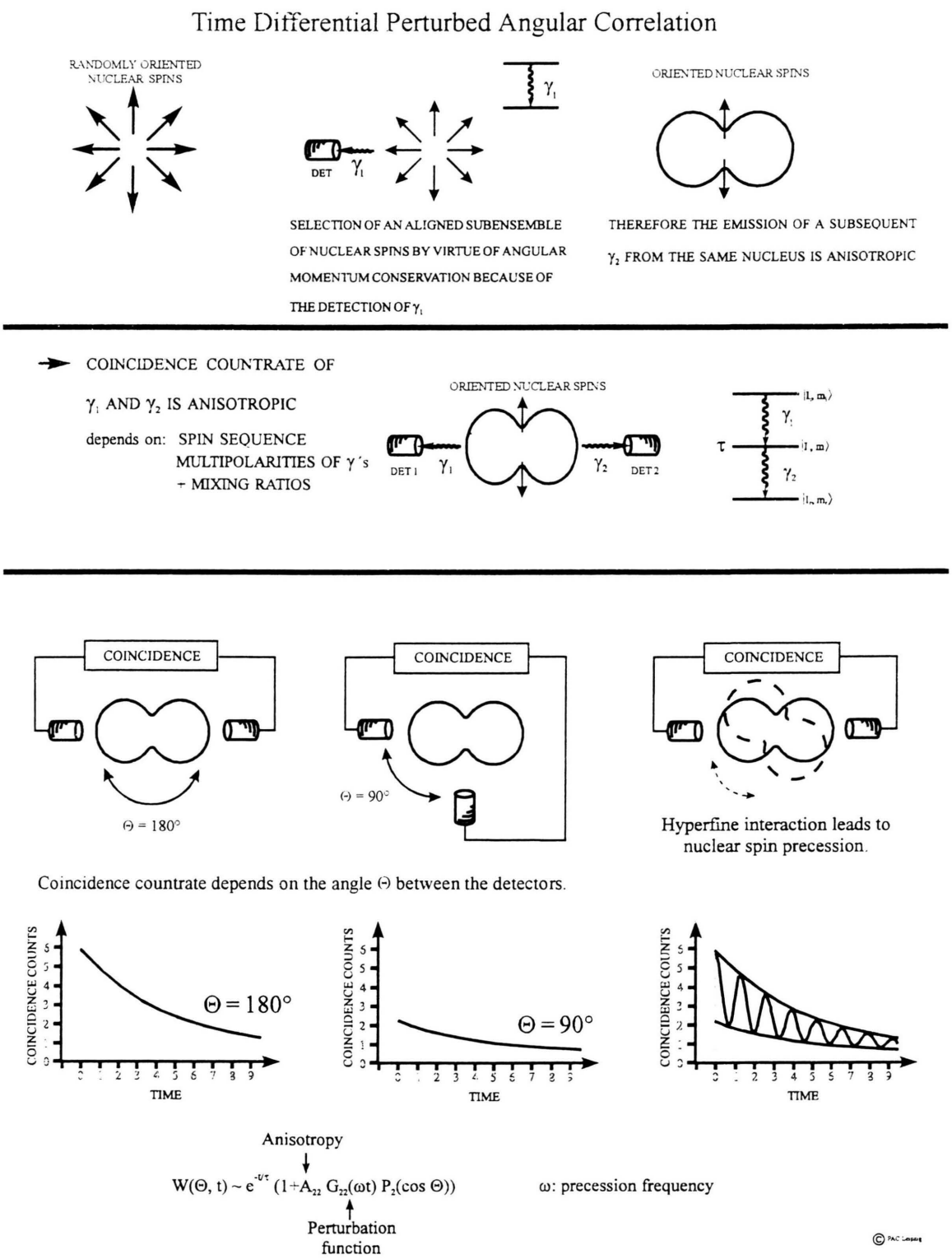

Fig. 2. Principles of TDPAC.

the intermediate level lifetime – the "exploration time" – is long enough, the coincidenc countrate pattern precesses in front of the detectors like the light cone in a lighthouse. A nucleus that happens to emit γ_2 immediately after the population of the intermediate state by the γ_1 transition (i.e. a prompt coincidence) will contribute to an unperturbed correlation because it had no time to precess. On the other hand, a nucleus that emits γ_2 one quarter of the precession period later than γ_1 will contribute to the angular correlation as if the detectors were at $\theta = 90°$. Hence, a time differential recording of delayed coincidence events is required in order to avoid averaging over the various nuclei which have precessed to various extents. This situation is depicted in Fig. 2, bottom. A coincidence histogram is recorded as a function of the time elapsed between the emission of γ_1 and γ_2. For unperturbed systems (e.g., no electric field gradient) we would have different coincidence countrates for detectors 180° or 90° apart, both decaying exponentially with τ_N, i.e. we perform a lifetime measurent. For a precessing nucleus, we would measure a modulated exponential decay curve for detectors fixed at 180°. The spin precession leads to an oscillation between both extremes at 180° and 90°. This modulated exponential decay resembles very closely the free induction decay in pulsed NMR. In fact, the modulation – called perturbation for historical reasons – contains all relevant information on the hyperfine-spilt intermediate level. It is common practice to Fourier transform this perturbation function in order to recover the energy (or frequency) splittings of the hyperfine split state.

3. TDPAC – Quantitative Formulation

a) Unperturbed Angular Correlation

The coincidence countrate for the two γ-rays emitted into the directions $\boldsymbol{k}_1$ and $\boldsymbol{k}_2$ can be written in the form [1, 2]

$$W(\boldsymbol{k}_1, \boldsymbol{k}_2) \propto \sum_{m_i, m_f} \sum_{m, m'} \langle m_f | \mathbf{H}_2 | m \rangle \langle m | \mathbf{H}_1 | m_i \rangle \cdot \langle m_f | \mathbf{H}_2 | m' \rangle^* \langle m' | \mathbf{H}_1 | m_i \rangle^* . \quad (1)$$

Here, the matrix element of the operator $\mathbf{H}_1$, which describes the interaction between the nucleus and the radiation field of γ_1, is taken between the initial states m_i and the intermediate states m (from right to left!), followed by the corresponding matrix element of $\mathbf{H}_2$ for γ_2 between the same intermediate states m and the final states m_f. In order to obtain an observable probability, the complex conjugated matrix elements enter as well. Since none of the sublevels m_i, m, or m_f is observed separately, we have to sum over all. The angular part of these matrix elements can be factored out using the Wigner-Eckart theorem. From (1) we then arrive at the expression

$$W(\boldsymbol{k}_1, \boldsymbol{k}_2) \propto \sum_{k_1 k_2 N_1 N_2} A_{k_1}(1) A_{k_2}(2) \cdot \frac{1}{\sqrt{2k_1+1)(2k_2+1)}} Y_{k_1}^{N_1^*}(\theta_1, \phi_1) Y_{k_2}^{N_2}(\theta_2, \phi_2) \quad (2)$$

with

$$A_k(1) = F_k(L_1 L_1 I_i I) = (-1)^{I_i + I - 1}(2L_1+1) \cdot \sqrt{(2I+1)(2k+1)} \begin{pmatrix} L_1 & L_1 & k \\ 1 & -1 & 0 \end{pmatrix} \begin{Bmatrix} L_1 & L_1 & k \\ I & I & I_i \end{Bmatrix},$$

$$A_k(2) = F_k(L_2 L_2 I_f I) = (-1)^{I_f + I - 1}(2L_2+1) \cdot \sqrt{(2I+1)(2k+1)} \begin{pmatrix} L_2 & L_2 & k \\ 1 & -1 & 0 \end{pmatrix} \begin{Bmatrix} L_2 & L_2 & k \\ I & I & I_f \end{Bmatrix}.$$

Here, $Y_k^N(\theta_i, \phi_i)$ is a spherical harmonic with θ_i and ϕ_i denoting the polar and azimuthal angles of the vector $\boldsymbol{k}_i$. The symbols in the definition of the A_k are vector coupling coefficients, namely Wigner 3j- and 6j-symbols. They can be found in [3]. The F_k-coefficients are tabulated in [1] or [4]. For transitions with mixed multipolarities, the A_k consist of F_k-coefficients for both pure multipolarities and a mixing term (for further details cf. [4]). The k_1 and k_2 on the right hand side of (2) are summation indices which run from 0 to $k_{\max}$ in steps of 2 (even parity!). Here, $k_{\max} = \min(2L_1, 2L_2, 2I)$ with L_1, L_2 being the (lowest) multipolarity of γ_1 and γ_2 and I denoting the intermediate state spin. The indices $N_{1,2}$ run from $-k_{1,2}$ up to $+k_{1,2}$ in steps of 1. The sum over $N_{1,2}$ in (2) can be performed using the addition theorem for spherical harmonics:

$$\sum_N Y_k^{N^*}(\theta_1, \phi_1) Y_k^N(\theta_2, \phi_2) = (2k+1) P_k(\cos\theta). \quad (3)$$

$P_k(\cos\theta)$ denotes the Legendre polynomial with θ being the angle between the vectors $\boldsymbol{k}_1$ and $\boldsymbol{k}_2$:

$$\cos\theta = \cos\theta_1 \cos\theta_2 + \sin\theta_1 \sin\theta_2 \cos(\phi_1 - \phi_2). \quad (4)$$

With the help of (3) we finally arrive at the unperturbed angular correlation function

$$W(\boldsymbol{k}_1, \boldsymbol{k}_2) = W(\theta) = \sum_k A_k(1) A_k(2) P_k(\cos\theta). \quad (5)$$

To lowest order we have

$$W(\theta) \propto 1 + A_2(1)\,A_2(2)\,P_2(\cos\theta) = 1 + A_{22}(3/2\cos^2\theta - 1/2). \quad (6)$$

Here, A_{22} (the anisotropy) is a shorthand for $A_2(\gamma_1)\,A_2(\gamma_2)$.

Suppose that the intermediate state has a finite lifetime τ_N but that we explicity *exclude* any interaction, which could lead to a precession while the nucleus is in the intermediate level. We would then have a time-dependent coincidence countrate

$$W(\theta, t) \propto \exp\left(\frac{-t}{\tau_N}\right)\sum_k A_{kk}\,P_k(\cos\theta) \quad (7)$$

which decays exponentially with the lifetime τ_N but leaves the angular correlation unperturbed, i.e. there is no time dependence in the angular part. The time integrated countrate would equal (5). This situation, of course, is only of interest to nuclear physicists who extract information on nuclear spins and multipolarities of transitions. In the following we assume that the quantities A_{kk} and τ_N, are all well-known.

b) Perturbed Angular Correlation

If the nucleus in its intermediate excited level interacts with extranuclear perturbing fields, a mixing of intermediate states, say from m_a *after* γ_1 to a new state m_b *before* γ_2, occurs which is described by the evolution operator $\hat{\Lambda}(t)$:

$$W(\boldsymbol{k}_1, \boldsymbol{k}_2, t) \propto \exp\left(\frac{-t}{\tau_N}\right)\sum_{m_i, m_f}\sum_{m_a, m_b}\sum_{m_{a'}, m_{b'}} \cdot\langle m_f|\mathbf{H}_2|m_b\rangle\langle m_b|\hat{\Lambda}(t)|m_a\rangle\langle m_a|\mathbf{H}_1|m_i\rangle \quad (8)$$
$$\cdot\langle m_f|\mathbf{H}_2|m_{b'}\rangle^*\langle m_{b'}|\hat{\Lambda}(t)|m_{a'}\rangle^*\langle m_{a'}|\mathbf{H}_1|m_i\rangle^*.$$

The coincidence countrate of (2) is now modified to account for this mixing:

$$W(\boldsymbol{k}_1, \boldsymbol{k}_2, t) \propto \exp\left(\frac{-t}{\tau_n}\right)\sum_{k_1 k_2 N_1 N_2} A_{k_1}(1)\,A_{k_2}(2)\,G_{k_1 k_2}^{N_1 N_2}(t) \cdot\frac{1}{\sqrt{(2k_1+1)(2k_2+1)}}\,Y_{k_1}^{N_1^*}(\theta_1, \phi_1)\,Y_{k_2}^{N_2}(\theta_2, \phi_2) \quad (9)$$

with the perturbation function

$$G_{k_1 k_2}^{N_1 N_2}(t) = \sum_{m_a m_b}(-1)^{2I+m_a+m_b}\sqrt{(2k_1+1)(2k_2+1)} \cdot\langle m_b|\hat{\Lambda}(t)|m_a\rangle\langle m_{b'}|\hat{\Lambda}(t)|m_{a'}\rangle^* \cdot\begin{pmatrix} I & I & k_1 \\ m_{a'} & -m_a & N_1\end{pmatrix}\begin{pmatrix} I & I & k_2 \\ m_{b'} & -m_b & N_2\end{pmatrix}.$$

The primed quantities in the 3j-symbols of the perturbation function are defined via the sum-rule for 3j-symbols: the sum of the bottom row elements has to add up to zero. Suppose, the evolution operator $\hat{\Lambda}(t)$ is diagonal and expressed in terms of the eigenvalues E_m of the perturbing Hamiltonian:

$$\langle m_b|\hat{\Lambda}(t)|m_a\rangle = \exp\left(\frac{-i}{\hbar}E_m t\right)\delta_{mm_a}\delta_{mm_b}. \quad (10)$$

The perturbation function then simplifies to

$$G_{k_1 k_2}^{N N}(t) = \sum_m(-1)^{2I+m_a+m_b}\sqrt{(2k_1+1)(2k_2+1)} \cdot\begin{pmatrix} I & I & k_1 \\ m' & -m & N\end{pmatrix}\begin{pmatrix} I & I & k_2 \\ m' & -m & N\end{pmatrix}\exp\left\{\frac{-i}{\hbar}(E_m - E_{m'})t\right\}. \quad (11)$$

Note that in this case $N_1 = N_2 = N$. This diagonal situation would arise for magnetic dipole interactions and for axially symmetric electric quadrupole interactions.

For non-axially symmetric quadrupole interactions we require a unitary matrix $\mathbf{U}$ which diagonalizes the Hamiltonian $\mathbf{H}$:

$$\mathbf{U}^{-1}\mathbf{H}\,\mathbf{U} = \mathbf{D}, \quad (12)$$

where $\mathbf{D}$ is the diagonal matrix with eigenvalues E_m. Instead of (11) we then have

$$G_{k_1 k_2}^{N_1 N_2}(t) = \sum_{m_a m_b}(-1)^{2I+m_a+m_b}\sqrt{(2k_1+1)(2k_2+1)} \cdot\begin{pmatrix} I & I & k_1 \\ m_{a'} & -m_a & N_1\end{pmatrix}\begin{pmatrix} I & I & k_2 \\ m_{b'} & -m_b & N_2\end{pmatrix} \cdot\sum_{mm'}\langle m_b|m\rangle^*\langle m_a|m\rangle\langle m_{b'}|m'\rangle\langle m_{a'}|m'\rangle^* \cdot\exp\left\{\frac{-i}{\hbar}(E_m - E_{m'})t\right\}, \quad (13)$$

where $\langle i, j\rangle$ are the matrix elements of $\mathbf{U}$. The sum over m, m' describes the mixing of the sublevels due to the broken axial symmetry. In the following, we further simplify the perturbation functions restricting ourselves to randomly oriented samples ("microcrystals", "molecules", "powders"), i.e. we average over the Euler angles describing the quantization axis in each microcrystal with respect to the laboratory coordinate system in which $\boldsymbol{k}_1$ and $\boldsymbol{k}_2$ (emission directions) are defined.

This leads to the condition $k_1 = k_2 = k$ and $N_1 = N_2 = N$ (even for non-axial symmetry). The "powder" perturbation functions are then obtained as

a sum over certain "single crystal" perturbation functions:

$$G_{kk}(t) = \frac{1}{2k+1} \sum_{N=-k}^{k} G_{kk}^{NN}(t). \tag{14}$$

Since $G_{kk}(t)$ is independent of N, the addition theorem for spherical harmonics can again be applied and we obtain the "powder" angular correlation

$$W(\theta, t) \propto \exp\left(\frac{-t}{\tau_n}\right) \sum_k A_k(1)\, A_k(2)\, G_{kk}(t)\, P_k(\cos\theta). \tag{15}$$

For axial symmetry, the perturbation function of (14) can be rewritten:

$$G_{kk}(t) = \frac{1}{2k+1} + \sum_{m \neq m'} \begin{pmatrix} I & I & k \\ m' & -m & N \end{pmatrix}^2 \cos\frac{(E_m - E_{m'})t}{\hbar}. \tag{16}$$

Note that there is a time-independent contribution $1/(2k+1)$ in (16). This term is called the "hardcore" for historical reasons: in time integral perturbed angular correlations all oscillatory terms average out to zero for sufficiently high precession frequencies, but a certain fraction of the anisotropy (for $k=2: A_{22}/5$) remains, irrespective of the strength of the interaction. This hardcore is affected by fluctuating NQI's only, not by static inhomogeneous NQI-distributions. Hence, the hardcore offers an unambiguous discrimination between dynamic and static inhomogeneous line broadening.

In the next section we shall discuss NQI's for $I = 1$, 3/2, 2, 5/2, and 9/2 and give examples for powder perturbation functions and their Fourier transforms.

4. Perturbation Functions for NQI

The Hamiltonian for non-axially symmetric NQI's can be written as follows:

$$\begin{aligned} \mathscr{H}_{m,m} &= \hbar\omega_Q(3m^2 - I(I+1)), \quad \mathscr{H}_{m,m\pm1} = 0, \\ \mathscr{H}_{m,m\pm2} &= \hbar\omega_Q \eta \tfrac{1}{2}\sqrt{(I\mp m-1)(I\mp m)(I\pm m+1)(I\pm 2)} \end{aligned} \tag{17}$$

with $\omega_Q = -eQV_{zz}/(4I(2I-1)\hbar)$ and $\eta = (V_{xx} - V_{yy})/V_{zz}$. Here, V_{zz} is the largest component of the electric field gradient tensor (defined in its principal coordinate system, i.e. diagonal); V_{xx} and V_{yy} are the other two components which fullfill $V_{xx} + V_{yy} + V_{zz} = 0$. The nuclear quadrupole moment of the intermediate state is denoted by eQ. The asymmetry parameter η is in the range

$$0 \leq \eta \leq 1 \quad \text{if} \quad |V_{xx}| \leq |V_{yy}| \leq |V_{zz}|.$$

For $\eta = 0$, the Hamiltonian is already diagonal, and upon insertion of the eigenvalues (= diagonal elements) into (16) we finally arrive at

$$G_{kk}(t) = \frac{1}{2k+1} + \sum_{m \neq m'} \begin{pmatrix} I & I & k \\ m' & -m & N \end{pmatrix}^2 \cos(N\omega_L t), \tag{18}$$

where the summation sign means that the summation over m and m' should include these terms, where m and m' satisfy the condition

$$|m^2 - m'^2| = \begin{Bmatrix} N \\ 2N \end{Bmatrix} \quad \text{for} \quad I = \begin{Bmatrix} \text{integer} \\ \text{half-integer} \end{Bmatrix}. \tag{19}$$

Examples for various spins and $k=2$ are the following, displayed in Figure 3:

$$\begin{aligned}
I = 1: \quad & G_{22}(t) = \frac{3}{5} + \frac{2}{5}\cos\omega_0 t, && \omega_0 = 3\omega_Q; \\
I = \frac{3}{2}: \quad & G_{22}(t) = \frac{1}{5} + \frac{4}{5}\cos\omega_0 t, && \omega_0 = 6\omega_Q; \\
I = 2: \quad & G_{22}(t) = \frac{13}{35} + \frac{2}{35}\cos\omega_0 t + \frac{12}{35}\cos 3\omega_0 t + \frac{8}{35}\cos 4\omega_0 t, && \omega_0 = 3\omega_Q; \\
I = \frac{5}{2}: \quad & G_{22}(t) = \frac{7}{35} + \frac{13}{35}\cos\omega_0 t + \frac{10}{35}\cos 2\omega_0 t + \frac{5}{35}\cos 3\omega_0 t, && \omega_0 = 6\omega_Q; \\
I = \frac{9}{2}: \quad & G_{22}(t) = \frac{1}{5} + \frac{29}{165}\cos\omega_0 t + \frac{14}{165}\cos 2\omega_0 t + \frac{3}{11}\cos 3\omega_0 t + \frac{8}{55}\cos 4\omega_0 t \\
& \qquad + \frac{14}{165}\cos 5\omega_0 t + \frac{2}{55}\cos 7\omega_0 t, && \omega_0 = 6\omega_Q.
\end{aligned} \tag{20}$$

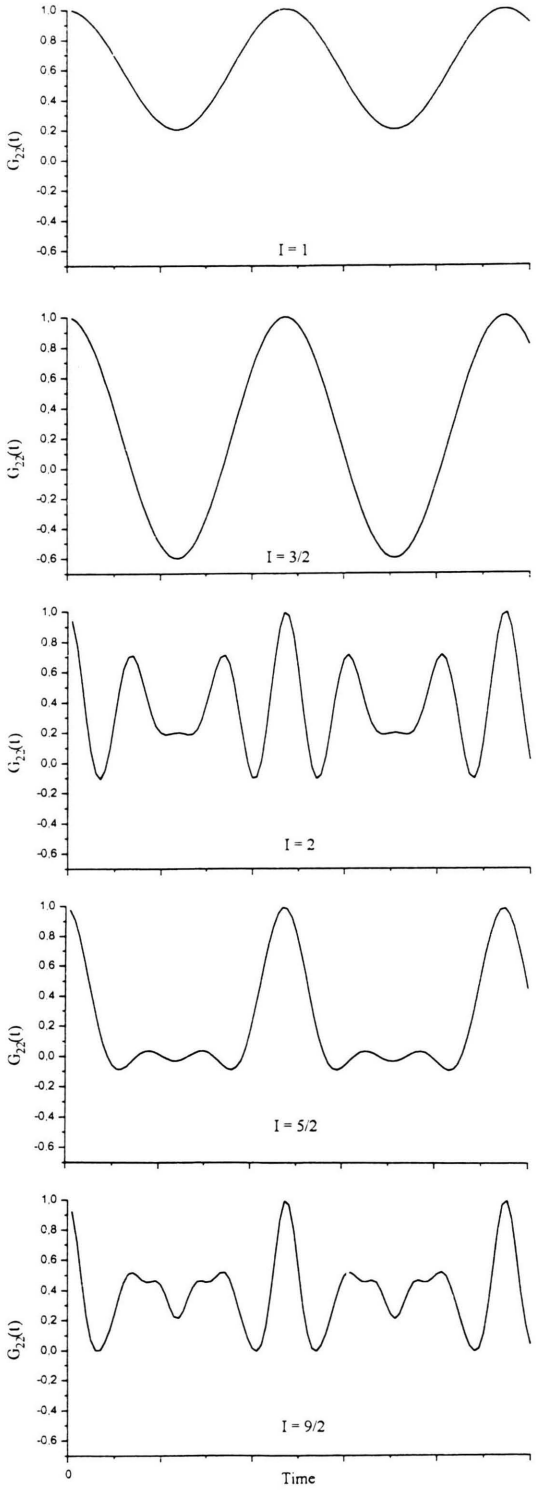

Fig. 3. Powder perturbation functions $G_{22}(t)$ for axial symmetry and various spins.

For $\eta \neq 0$ we have to diagonalize the Hamiltonian (17) and insert the eigenvalues into (13). Analytical expressions for the perturbation functions are derived in [5]. In Figs. 4a and 4b, the Fourier-transformed powder perturbation functions versus η are plotted for $I = 1$, 3/2, 2, 5/2, 9/2. In all cases, the perturbation functions are superpositions of undamped cosine-terms with η-dependent amplitudes and frequencies. Therefore all lines in Fig. 4 show the instrumental linewidth.

A finite additional linewidth can arise from a static frequency distribution. In this case, the cosine-terms should be multiplied by $\exp(-\frac{1}{2}\omega_i^2 \delta^2 t^2)$ or $\exp(-\omega_i \delta t)$ for Gaussian and Lorentzian distributions, respectively. Here, δ denotes the half width at half maximum (HWHM) of the distribution (for Lorentzians) or $\sqrt{2 \ln 2}$ times the HWHM (for Gaussians). Note that the hardcore is *not* changed, i.e. the peak at zero frequency has instrumental width irrespective of a static inhomogeneous broadening. This situation changes for fluctuating electric field gradients. For continuous isotropic reorientational motions, two simple limiting cases can be derived:

a) Slow relaxation limit [6] ($\omega \tau_C \gg 1$):

$$G_{22}(t) \approx e^{-t/\tau_C} G_{22}^{\text{static}}(t), \tag{21}$$

where $G_{22}^{\text{static}}(t)$ is either any of the functions discussed in (20) or modified versions thereof caused by a nonzero η. In the latter case, fluctuations in η are not taken into account. The reorientational correlation time is denoted by τ_C. Note that *all* lines including the hardcore are broadened to the same extent.

b) Fast relaxation limit [7]
(*Abragam-Pound limit*; $\omega \tau_C \ll 1$):

$$G_{22}(t) = e^{-\gamma t} \quad \text{with} \quad \gamma = \frac{18}{5} \tau_C \omega_Q^2 (4I(I+1) - 7). \tag{22}$$

In this case, only the product $\tau_C \omega_Q^2$ can be extracted from a measured spectrum. This exponential loss of the anisotropy is intuitively plausible, but it is certainly incorrect in the limit $t \to 0$. A finite slope at $t = 0$ implies a *finite* action in an *infinitely* short time which is impossible for finite ω_Q.

Discrete relaxation models that include a number of discrete classical states are best treated in the Liouville superoperator formalism. In general, no closed-forms for the perturbation functions can be given. We conclude this section by quoting a simple case of a system fluctuating between two different classical ($\eta = 0$) states *without* reorientation. This is the classical mo-

tional narrowing result in the time domain: the factor $\exp(izt)$ with $z = -3(m^2-m'^2)$ in (11) has to be replaced by [8]

$$e^{-\bar{\gamma}t+iz\bar{\omega}t}\left[\cosh(at)+\left(\bar{\gamma}-\frac{iz(\Delta\omega)(\Delta\gamma)}{\bar{\gamma}}\right)\frac{\sinh(at)}{a}\right]$$

with

$$\bar{\gamma}=\frac{\gamma_{\mathrm{I}}+\gamma_{\mathrm{II}}}{2},\quad \Delta\gamma=\frac{\gamma_{\mathrm{I}}-\gamma_{\mathrm{II}}}{2},\quad z=-3(m^2-m'^2),\quad \bar{\omega}=\frac{\omega_Q^{\mathrm{I}}+\omega_Q^{\mathrm{II}}}{2},\quad \Delta\omega=\frac{\omega_Q^{\mathrm{I}}-\omega_Q^{\mathrm{II}}}{2}, \tag{23}$$

$$a_0=iz\bar{\omega}-\bar{\gamma},\quad \alpha_x=\bar{\gamma},\quad a_y=i\Delta\gamma,\quad a_z=iz\Delta\omega-\Delta\gamma,\quad a=\sqrt{a_x^2+a_y^2+a_z^2}.$$

The limiting cases are easily derived:

$$\begin{aligned}&\text{a)}\quad \bar{\gamma}\to 0,\ \frac{\Delta\gamma}{\bar{\gamma}}\to 0: && \frac{1}{2}(e^{iz\omega_{\mathrm{I}}t}+e^{iz\omega_{\mathrm{II}}t}) && \text{“static superposition”},\\ &\text{b)}\quad \bar{\gamma}^2\gg z^2\Delta\omega^2,\ \bar{\gamma}\gg z\Delta\omega\Delta\gamma: && e^{iz\bar{\omega}t} && \text{“complete motional narrowing”}.\end{aligned} \tag{24}$$

Note that the hardcore remains unaffected, because for $z = 0$, (23) reduces to unity. It is not affected by the fluctuating electric field gradient because there is *no* reorientation involved.

Perturbation functions for single crystals are discussed in [5]. The precession frequencies are unaffected, of course, but the intensities of the various cosine-terms in this case depend on the orientation of the quantization axis with respect to the detectors. For single crystals, it is also possible to derive – apart from V_{zz} and η – the three Euler angles that describe the orientation of the quantization axis with respect to k_1 and k_2.

5. TDPAC-Spectrometers

It is clear that TDPAC spectrometers should fulfill the following requirements:

a) proper choice of the detectors for the γ-quanta involved;
b) high detection efficiency is imperative because we are dealing with *coincidence* measurements rather than single counts;
c) large solid angles per detector progressively wipe out the angular part of the perturbation function. Hence, multi-detector arrangements are preferable;
d) the energy resolution of the detectors should be sufficiently good to distinguish between γ_1 and γ_2 and possibly between other decay-quanta not associated with the cascade of interest;
e) the time resolution for the detection of the delayed coincidence histogram should also be as good as possible, preferably better than 1 ns.

All spectrometers use two separate circuits to accomplish these tasks: the “slow”-circuit for the energy discrimination and the “fast”-circuit for the timing. Rather then to discuss all possibilities, we present a schematic circuit for a modern 6-detector setup only. In Fig. 5, the sample is surrounded by 6 detectors. In reality, they are arranged in a cube such that there are three pairs facing each other (i.e. 6 combinations with $\theta = 180°$ and 24 combinations with $\theta = 90°$). Each detector consists of a conically shaped BaF_2 scintillator mounted on an XP2020Q photomultiplier tube with a quartz window. Each covers about 10% of 4π solid angle. The dynode (energy) signal is amplified and selected using single channel analysers for γ_1 or γ_2. The anode (timing) signal is delayed until the energy signals are available for further processing. The routing/coincidence unit serves two purposes:

(i) in acts as a fast switch for the timing signal, which is either directed to the start output (if coincident with the logic signal for γ_1), to the stop output (if coincident with the logic signal for γ_2), or discarded.
(ii) it checks for overlap within the region of interest of pulses for γ_1 and detector i with pulses for γ_2 and detector j and creates an address for the multichannel analyser (MCA) subgroups corresponding to W_{ij}.

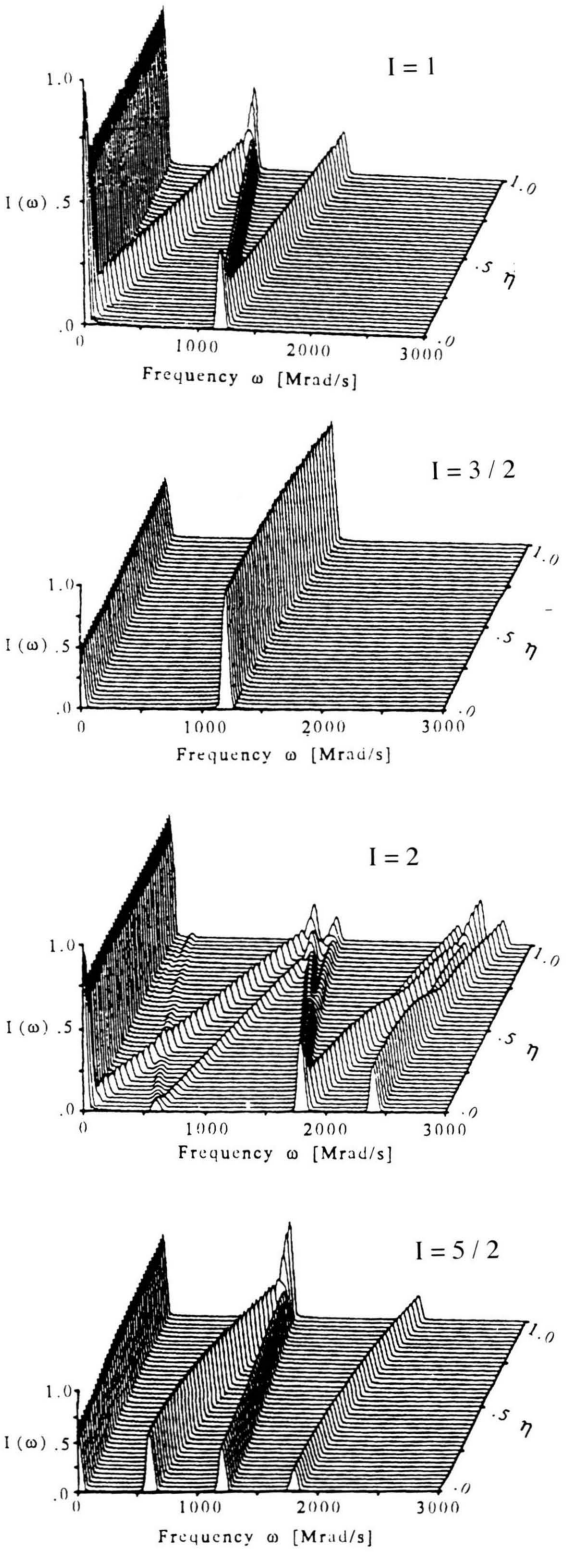

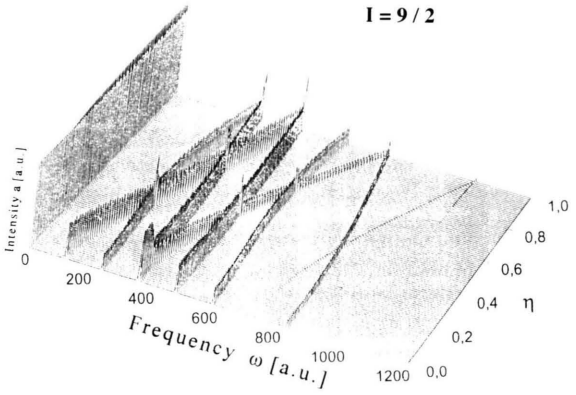

Fig. 4. Stacked plot of Fourier transformed powder perturbation functions $G_{22}(t)$ as a function of the asymmetry parameter η for nuclear spins $I = 1$, 3/2, 2, 5/2, and 9/2.

The time difference between start and stop pulses is determined accurately by a combination of a time to amplitude and an amplitude to digital converter (this may also be combined into a time to digital converter).

The 30 possible detector combinations are stored simultaneously in 30 MCA subgroups. They are combined in the following way (after subtraction of accidental background and shift to a common time origin):

$$R(t) = 2\,\frac{W(180°) - W(90°)}{W(180°) + 2\,W(90°)}$$

with (25)

$$W(180°) = \sqrt[6]{\text{Product of all 6 } 180°\text{-combinations}},$$

$$W(90°) = \sqrt[24]{\text{Product of all 24 } 90°\text{-combinations}}.$$

In this ratio, the exponential decay factors cancel and the detector efficiencies are eliminated to first order. For powder samples and $k = 2$, (25) reduces to $R(t) = A_{22}\,G_{22}(t)$. This is usually called the TDPAC time spectrum.

6. TDPAC-Isotopes

Table 1 contains a collection of isotopes that can be used for γ-γ-TDPAC in NQI-research. It is by no means complete. The following quantities are listed, taken from [9]: mother isotope,– decay type, – daughter isotope, – intermediate level spin I, half life $\tau_{1/2}$,

Table 1. Properties of typical TDPAC-Isotopes.

Mother isotope	Decay	Daughter isotope	Intermediate state			Cascade [keV]	A_{22}^{max} [%]	FOM* [ns · b]
			I	$\tau_{1/2}$ [ns]	Q [b]			
^{44}Ti	EC	^{44}Sc	1^+	153 (1)	+0.21 (2)	78–68	+ 4.5 (3)	0.33
^{57}Co	EC	^{57}Fe	$3/2^-$	98.5 (8)	+0.082 (8)**	122–14.4	+ 2.3 (3)	0.021
^{99}Mo	β^-	^{99}Tc	$5/2^+$	3.61 (7)	±0.3?	740–(40)–141	−12.4 (5)	0.083?
^{99}Mo	β^-	^{99}Tc	$5/2^+$	3.61 (7)	±0.3?	740–181	+10.0 (6)	0.054?
^{99}Rh	EC	^{99}Ru	$3/2^+$	20.5 (1)	+0.34 (7)***	527–89	−22.1 (20)	1.7
^{100}Pd	EC	^{100}Rh	2^+	214.5 (20)	±0.076 (20)	84–75	+16 ( )	2.1
^{111}Ag	β^-	^{111}Cd	$5/2^+$	84.5 (5)	+0.83 (13)	95.5–245	−13 ( )	5.9
^{111m}Cd	IT	–	$5/2^+$	84.5 (5)	+0.83 (13)	150–245	+16 ( )	9.0
^{111}In	EC	^{111}Cd	$5/2^+$	84.5 (5)	+0.83 (13)	171–245	−18.0 (2)	11.4
^{115}Cd	β^-	^{115}In	$3/2^+$	5.78 (6)	−0.60 (2)	35–492	+20.9 (2.4)	0.76
^{117}Cd	β^-	^{117}In	$3/2^+$	53.6 (7)	−0.59 (1)	89–345	−36 ( )	20.5
^{118m}Sb	EC	^{118}Sn	5^-	22 (5)	+0.16 (2)	245–1050/1229	+10.7 (9)	0.20
^{129m}Te	β^-	^{129}I	$5/2^+$	16.8 (2)	−0.68 (5)	460–28	− 5.1 (9)	0.15
^{133}Ba	EC	^{133}Cs	$5/2^+$	6.30 (2)	−0.33 (2)	356–81	+ 3.61 ( )	0.014
^{140}La	β^-	^{140}Ce	4^+	3.45 (9)	+0.35 (7)	329–487	−13.2 (15)	0.11
^{127}Lu	EC	^{172}Yb	3^+	8.1 (2)	+2.87 (41)	91–1094	+33.0 (13)	12.7
^{181}Hf	β^-	^{181}Ta	$5/2^+$	10.8 (1)	+2.36 (5)	133–482	−28.9 (11)	10.6
^{187}W	β^-	^{187}Re	$9/2^+$	555 (2)	+3.04 (5)	479–72	−12 (3)****	121
^{199m}Hg	IT	–	$5/2^-$	2.45 (5)	+0.95 (7)	374.1–158.4	+18.4 (6)	0.39
^{204m}Pb	IT	–	4^+	265 (10)	+0.44 (2)	912–375	+22 (1)	28.2

* FOM = $5\,\tau_{1/2}\,(A_{22}^{exp})^2\,|Q|$.
** Other reported $Q = 0.16$ b [17].
*** Other reported $Q = +0.231$ (12).
**** Due to an admixture of x-rays in the stop $\gamma_2 = 72$ keV A_{22} is normally much smaller.

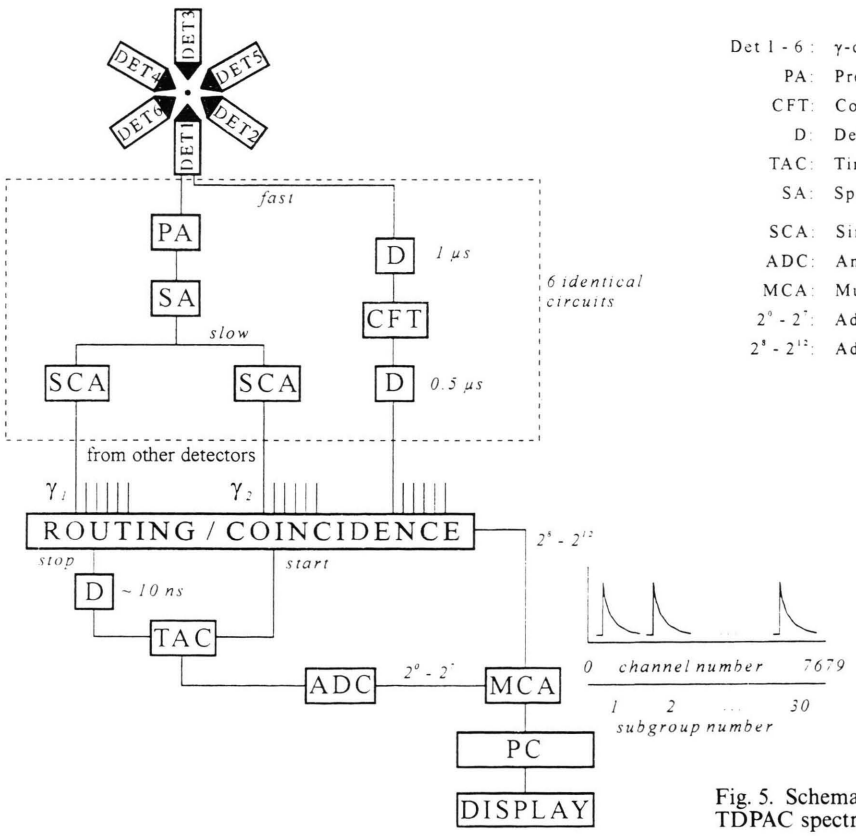

Det 1 - 6: γ-detectors
PA: Preamplifier
CFT: Constant fraction trigger
D: Delay
TAC: Time to amplitude converter
SA: Spectroscopy amplifier
SCA: Single channel analyser
ADC: Analog to digital converter
MCA: Multichannel analyser
2^0 - 2^7: Address bits for histogram
2^8 - 2^{12}: Address bits for subgroups

Fig. 5. Schematic block diagram of a 6-detector TDPAC spectrometer.

quadrupole moment Q, – cascade energies, – maximum experimental anisotropy A_{22}^{max}, – figure of merit (FOM).

This FOM is somewhat arbitrarily defined as

$$\text{FOM} = 5 \cdot \tau_{1/2}(A_{22}^{max})^2 \cdot |Q|. \quad (26)$$

The reasoning is the following: usually some 5 halflives can be recorded (for longer delays the signal to noise ratio becomes too poor) and the product of this time window with the "signal" $(A_{22}^{max})^2$ defines the "information" in the sense of Parsevals theorem. This quantity is multiplied by $|Q|$ in order to incorporate an NQI specific ingredient. No other suitability factors such as low branching ratios for the cascade, high spins, interfering γ-rays, high conversion coefficients, mother isotope production problems, mother isotope lifetime and alike enter the FOM. Nevertheless, it serves the purpose to give a quick overview.

Numbers in brackets denote uncertainties in the last digit(s) (if unknown, an empty bracket is quoted).

According to Table 1, based on the FOM, ^{187}W should be an exceptionally well suited isotope. However, in practice it is rarely used. The reason is the fact that $A_{22}^{max} = -12\%$ is only achievable if the 72-keV γ-line and the x-ray lines are well separated, which is only partly possible with high-resolution semiconductor detectors. ^{204m}Pb and ^{117}Cd are also not widely used. The reasons are probably the short halflife and the high spin for ^{204m}Pb. ^{111}In is probably the "^{57}Fe" of the TDPAC community, ^{181}Hf is also widely in use. ^{172}Lu is not used to a larger extent because the branching ratios are low, the number of interfering γ-rays is high, and it is difficult to produce.

All these isotopes are either commercially available or they have to be produced by nuclear reactions such as thermal neutron capture, cyclotron irradiations, or fission, fragmentation, or spallation followed by isotope separation. They are frequently available "carrier-free". The incorporation into the molecule or solid of interest can be performed in a variety of ways: during synthesis, by implantation (including recoil implantation), or by irradiation of the sample, i.e. the nuclear reaction takes place *in* the sample (and side reactions should be minimized). These latter two methods introduce radiation damage and annealing procedures are frequently required. The following situations are encountered:

a) The probe atom has a longlived isomeric state and is a natural constituent of the sample. In this case, there are no problems with the substitutional incorporation of the "spy". The interpretation of the NQI results is straightforward.
b) The mother isotope is a constituent of the sample, but its daughter is not. In this case, no preparative difficulties arise, but the daughter isotope, on which the NQI is determined, is a foreign atom. This means, that there could be electronic or chemical "after-effects" following the nuclear transmutation. The interpretation of the NQI data is less straightforward because there might be impurity specific features.
c) The daughter isotope is a constituent of the sample, but the mother is not. Here, preparative problems could arise because we are now dealing with "doping" with impurity atoms. Once this question is answered – either the probe is substitutional or the lattice site is known – we have to discuss the possibility that after-effects might take place. However, usually the electronic and lattice rearrangement is fast enough to render after-effects unlikely, especially in the case of transmutation into a constituent atom. There are in general no interpretation problems.
d) Neither the mother nor the daughter isotope is a constituent of the sample. In this case, all possible complications mentioned above can arise.

This list of situations is biased by applications where the NQI at a certain lattice site (or site in a molecule) is of interest, preferably of a constituent atom. There are, however, a large number of applications where a foreign atom at "infinite dilution" is introduced on purpose and where impurity-defect or impurity-impurity interactions are studied intentionally. In these cases, the doping conditions have to be optimized and lattice location studies are indispensible.

7. Examples

In this section, two modern examples are given that illustrate to some extent "extreme" cases: applications using ^{199m}Hg with a rather short $\tau_{1/2}$ and a poor FOM and ^{187}W with a very long $\tau_{1/2}$ and a good FOM.

a) Two- and Four-Fold Coordination of Hg by S

^{199m}Hg was produced by thermal neutron capture using enriched ^{198}HgO which was subsequently dis-

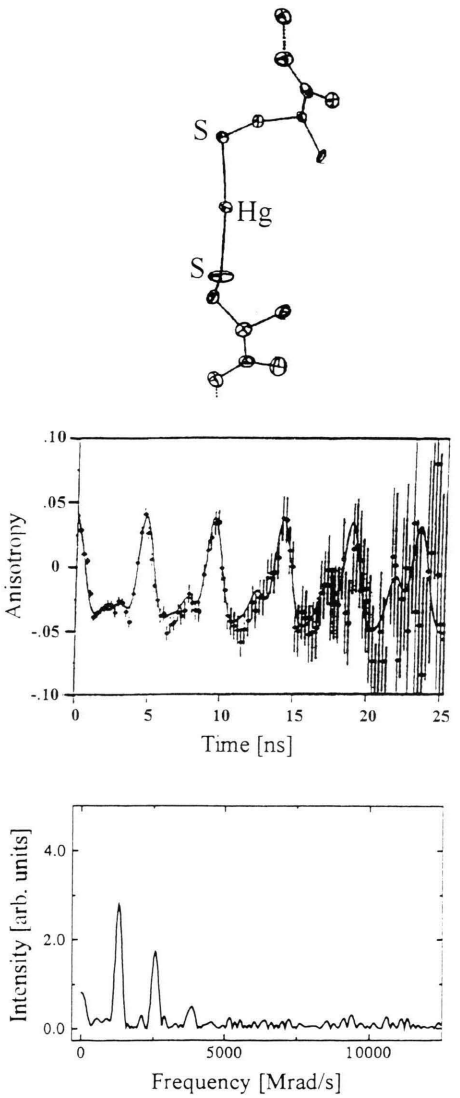

Fig. 6. Structure of Hg (cysteine)$_2$, TDPAC time spectrum for ^{199m}Hg (cys)$_2$, and corresponding Fourier transform (from top to bottom) at room temperature.

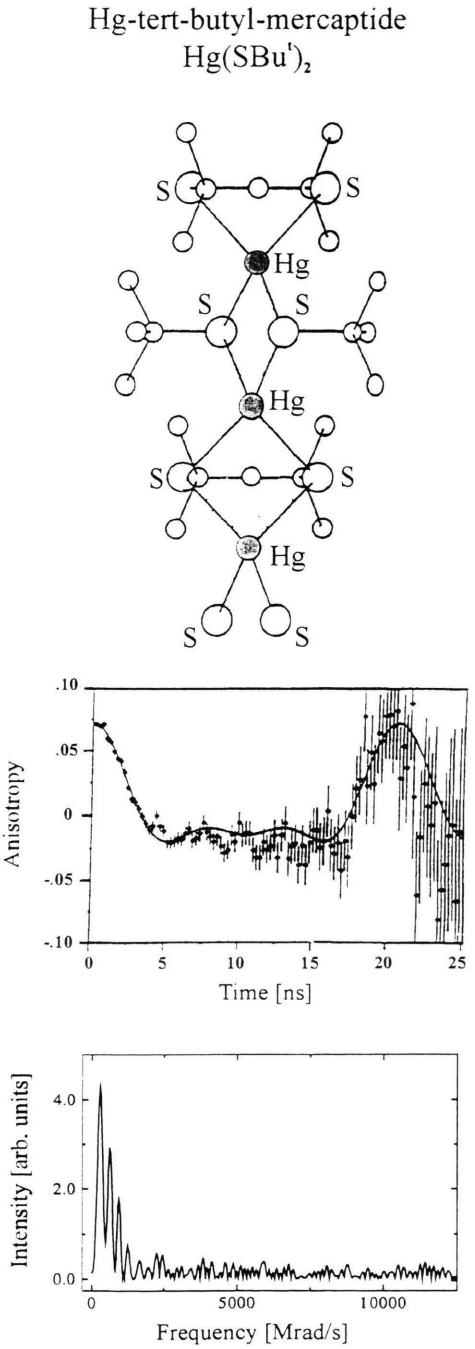

Fig. 7. Structure of Hg-tert-butyl-mercaptide, TDPAC time spectrum for ^{199m}Hg (sBu)$^t_2$, and corresponding Fourier transform (from top to bottom) at room temperature.

See [10] for references referring to structure determinations.

solved in acetic acid. The Hg compounds were produced by standard chemical techniques. Hg has a strong preference for two-fold coordination, especially with S ligands. For identical ligands and an isolated molecule, a linear bond with a 180° bond angle is expected. In the condensed state, deviations from 180° occur as a result of intermolecular interactions or distant counterions. In general, the NQI should be large and close to axially symmetric. The *p*-orbitals of both ligands contribute an equal amount to the electric field gradient, and there is no cancellation caused by the collinearity. A typical candidate is the complex formed with cysteine, as shown in Fig. 6, top. The observed TDPAC time spectrum and its Fourier transform are shown in Fig. 6, middle and bottom, respectively. The NQI is indeed large: $\nu_Q = e^2 q Q/h = 1.409(16)$ MHz; the deviation from axial symmetry is small: $\eta = 0.149(17)$ [10]. With $Q = 0.95$ b we obtain $V_{zz} = 6.13 \cdot 10^{18}$ V/cm^2, a rather large value.

Hg forms an unusual polymeric chain when reacted with tert-butyl-mercaptan, as shown in Fig. 7 (top). Hg is coordinated by 4 sulfur atoms in a distorted tetrahedral geometry. In this case, the *p*-orbitals with all sulfur ligands contribute (approximately) an equal amount to the electric field gradient, but there is a strong cancellation of individual contributions. In fact, for an undistorted regular tetrahedral coordination, the electric field gradient should vanish. Since the distortion is such that a two-fold rotation axis plus a mirror plane perpendicular to the chain axis and through the Hg position remains, the NQI is expected to be axially symmetric. Both expectations are confirmed by experiment (see Fig. 7, middle and bottom). The NQI is low: $\nu_Q = 353(4)$ MHz, $\eta = 0$ [10]. With $Q = 0.95$ b we derive $V_{zz} = 1.54 \cdot 10^{18}$ V/cm^2. Detailed ab initio calculations of the NQI should be feasible for both compounds, as demonstrated for the Hg-halides [11], although the computational effort is significantly larger because of the large number of atoms in the unit cell.

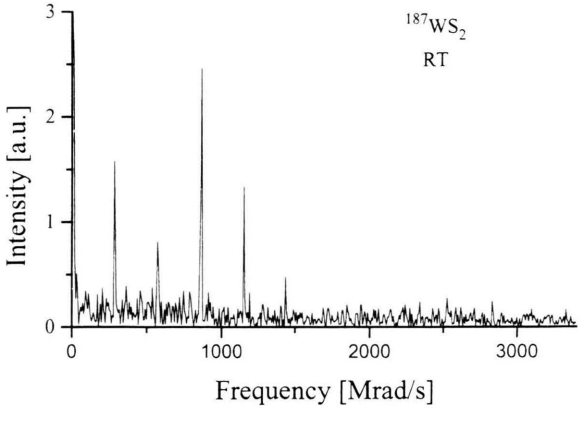

Fig. 8. Fourier transformed TDPAC spectrum for $^{187}WS_2$ at room temperature.

b) The NQI of ^{187}Re in WS_2

The mother isotope ^{187}W of ^{187}Re was produced in WS_2 single crystals via thermal neutron capture by irradiating them in a nuclear reactor. Subsequently, the crystals were annealed at 800 °C for 2 hours. Before the nuclear transmutation took place ^{187}W is undoubtedly on a W-site, therefore the mother isotope ^{187}Re should be substitutional, too. WS_2 is a layered compound with hexagonal slabs of W atoms sandwiched between two hexagonal slabs of S atoms. The S-W-S sandwiches are stacked on top of each other and held together by weak van-der-Waals interactions. There is a threefold rotation axis at the W site, hence the NQI should be axially symmetric. W is sixfold coordinated by S and also has six W neighbours. Since the sign of the electric field gradient is unknown, we can not speculate about the relative contribution of W-S and W-W orbitals. A previous study of WS_2 powder samples yielded $\nu_Q = 1083.31(42)$ MHz, $\eta = 0$ [12]. Figure 8 shows the Fourier transformed spectrum for a measurement performed on a WS_2 single crystal oriented along the body diagonal of the 6-detector cube arrangement. The observed precession frequency is identical to that of the previous study; but, because of the good time resolution in this recent experiment, all lines of the $I = 9/2$ pattern except the highest are observable. These lines are equidistant (with $\omega_6 = 6\,\omega_1$ missing), hence $\eta = 0$. The electric field gradient is not exceedingly large: with $Q = 3.04$ b we obtain $V_{zz} = 1.47 \cdot 10^{18}$ V/cm^2.

What is interesting in Fig. 8 is the rather narrow linewidth. We used 1024 channels per subgroup, i.e. a total of 32 K, with about 1 ns/channel. Hence, delayed coincidences for about 1 μsec were recorded only. With $\tau_{1/2} = 555$ ns, coincidences during a period of 2.5–3 μsec should be observable. This would require a memory with 128 K channels, not impracticable but unusual for TDPAC-work. The alternative would be to use a coarser time grid of say 4 ns/channels. In this case, however, one would loose all hamronics (they

would be above the Nyquist frequency). In any case, with more storage capacity, a linewidth about three times smaller should be achievable, provided the sample quality is high enough. In this case, also using a fast Fourier transform routine of 16 K or more input data is neccesary in order to avoid aliasing.

8. Conclusion

This tutorial paper serves two purposes: (a) it is useful as an introduction to researchers in the field of NQI's who are not familiar with TDPAC; to illustrate that working with excited nuclear states can be as exciting as working with ground states: (b) it is useful for TDPAC-experts as well, because the interest of the γ-ray spectroscopists with their individual photon detection devices have separated quite a bit from those of their collegues using RF-photons, coils, RF-pulses etc. The last example, namely ^{187}W-spectroscopy, provides a link from TDPAC towards NQR in several respects.

TDPAC spectroscopy is widely used by a growing community worldwide. Applications cover e.g. investigations of defects in metals and semiconductors, critical exponents in magnetically ordered materials, phase transitions in solids, interfaces, surfaces, intercalation and thermal decomposition reactions, diffusion in solids, and extend to biomolecules and radiopharmaceuticals. Those, who want to learn more about TDPAC, should refer to review articles [13–15]. A table of NQI's in metals obtained by nuclear spectroscopy on excited nuclear states was compiled by Vianden [16]. A similar table for compounds is given in [9].

It is a pleasure to thank Dr. W. Tröger and Mr. C. Lippert for their cooperation and help with the preparation of this manuscript.

[1] R. M. Steffen and H. Frauenfelder, in: Perturbed Angular Correlations, E. Karlsson, E. Matthias, and K. Siegbahn (eds.), North-Holland, Amsterdam 1964, p. 3–39.
[2] H. Frauenfelder and R. M. Steffen, in: Alpha-, Beta-, and Gamma-Ray Spectroscopy, K. Siegbahn (ed.), North-Holland, Amsterdam 1965.
[3] M. Rotenberg, R. Bivins, N. Metropolis, and J. K. Wooten, Jr., The 3-j and 6-j Symbols, Technology Press MIT, Cambridge, MA 1959.
[4] T. Yamazaki, Nuclear Data, Section A, Vol. 3, nr. 1, Academic Press, NY 1967, p. 1–23.
[5] T. Butz, Hyperfine Interact. **52,** 189 (1989); Erratum: Hyperfine Interact. **73,** 387 (1992).
[6] A. Abragam and R. V. Pound, Phys. Rev. **92,** 943 (1953).
[7] A. G. Marshall and C. F. Meares, J. Chem. Phys. **56,** 1226 (1972).
[8] W. Tröger and T. Butz, Z. Naturforsch. **47a,** 12 (1992).
[9] A. Lerf and T. Butz, Hyperfine Interact. **36,** 275 (1987); P. Raghavan, Atomic Data and Nuclear Data Tables **42,** 189 (1989).
[10] T. Butz, W. Tröger, Th. Pöhlmann, and O. Nuyken, Z. Naturforsch. **47a,** 85 (1992).
[11] W. Tröger, T. Butz, P. Blaha, and K. Schwarz, Hyperfine Interact. **80,** 1109 (1993).
[12] P. Mottner and T. Butz, Chem. Physics **147,** 199 (1990).
[13] H. H. Rinneberg, Atom. Energy Rev. **17,** 477 (1979).
[14] E. Recknagel, G. Schatz, and T. Wichert, in: Hyperfine Interactions of Radioactive Nuclei, J. Christiansen (ed.), Springer, Berlin 1983, p. 133.
[15] A. Lerf and T. Butz, Angew. Chemie, Int. Ed. Engl. **26,** 10 (1987).
[16] R. Vianden, Hyperfine Interact. **15/16,** 1081 (1983).
[17] Ph. Dufek, P. Blaha, and K. Schwarz, Phys. Rev. Lett. **75,** 3545 (1995).